TECHNICAL PAPER

A coupled thermo-mechanical model for the simulation of discrete particle systems

Osvaldo D. Quintana-Ruiz[1] · Eduardo M. B. Campello[1]

Abstract

This work presents a computational model for the simulation of problems involving thermo-mechanically active particles forming discrete particle systems. Our approach is based on the discrete element method for description of the particles' dynamics, combined with simple heat transfer equations to describe the various thermal effects that may take place when the system is excited by temperature gradients and external heat sources. We are able to track the motion of the particles and their thermal states over time under the influence of body (e.g., gravitational) forces, contact and friction forces (and the related moments w.r.t. the particles' centers), as well as applied heat from external devices, heat transfer through conduction (at the particles' interfaces upon contact with other particles and objects), convective cooling and radiative effects. Numerical examples are provided to validate our scheme and illustrate its applicability to the simulation of a wide range of engineering applications. We believe that simple, consistent particle models of the type as shown here may be a useful tool to the modeling of discrete particle systems that are consisted of thermo-mechanically active particles and, in a broader sense, many other multiphysical discrete systems.

Keywords Particles · Thermal effects · Coupled thermo-mechanics · Multiphysical particle systems · Discrete element method (DEM)

1 Introduction

In a variety of industrial processes and engineering applications, ranging from advanced manufacturing to state-of-the-art civil construction, the controlled heating and processing of thermo-mechanically active particles such as sintering powders and functionalized cementitious materials are of utmost importance. From a mechanistic point of view, these particles constitute discrete particle systems that may be subjected to a range of multiphysical effects, invariably including (but not restricted to) mechanical and thermal fields. Oftentimes, these effects are intrinsically interconnected, in the sense that the progress of one may affect the progress of the others, and vice versa, thus requiring a coupled physical

description for a reliable and accurate representation of the system's behavior. It is also common that the particles are functionalized, e.g., by reactive thin films adsorbed onto the particles' surface, which may be activated by inter-particle collisions and therefrom trigger chemical reactions. These reactions may be the source of additional heating or cooling to the system, which in turn may affect the thermo-mechanical behavior of the particles through added softening or stiffening of their base materials. Computational modeling of such discrete systems is quite recent in the literature (see, e.g., [1, 2]), and discrete particle simulation plays an important role in this regard. This technique yields an efficient analysis tool able to provide very rich information about the system at any desired time instant, such as the trajectories of (and transient forces acting on) individual particles, their individual temperatures (and heat flows and thermal powers), their detailed neighboring interactions, and many others, which are difficult (if not impossible) to obtain by conventional experimental techniques. Heat transfer in dry particle systems is often regarded to occur mostly through conduction, which in turn essentially depends on the conductivity of the particles' base material, the inter-particle

---

Technical Editor: Francis HR Franca, Ph.D.

✉ Eduardo M. B. Campello
  campello@usp.br

[1] Department of Structural and Geotechnical Engineering, University of São Paulo, P.O. Box 61548, São Paulo, SP 05424-970, Brazil

contacts and the structure of the particle packing. But other contributions, such as convective cooling and radiative effects, may likewise play an important role.

In this context, the purpose of this work is to present a simple, multiphysics computational model for the simulation of problems involving thermo-mechanically active particles forming discrete particle systems. Our approach is based on the discrete element method (DEM) for description the particles' dynamics, combined with simple (lumped) heat transfer equations to describe the various thermal phenomena that may take place when the system is excited by temperature gradients and external heat sources. We are able to track the motion of the particles and their thermal states over time under the influence of body (e.g., gravitational) forces, contact and friction forces (and the related moments w.r.t the particles' centers), as well as applied heat from external devices, heat transfer through conduction (at the particles' interfaces upon contact with other particles and objects), convective cooling and radiative effects. The model is relatively simple and straightforward to be implemented by engineers and analysts interested in the field and may be a useful tool for practical, rapid process simulation, design and analysis. Numerical examples are provided to validate our scheme and illustrate its applicability to the simulation of a wide range of engineering applications.

The DEM formulation adopted here follows from the work by Campello [3–5]. We will present it here in a summarized way, with the aim to provide just an overview of our discrete particle approach and introduce our notation. For a more detailed report, we refer the interested reader to the above-mentioned references. In general lines, our strategy to account for thermal effects into the DEM description follows the same ideas as those of Zohdi [6, 7], whose works are, in our opinion, the pioneering successful attempts to the modeling and computational simulation of discrete particle systems with temperature effects for modern engineering applications. It differs from Zohdi's approach, however, in the sense that (1) we adopt a fully consistent stick–slip friction model for arbitrarily rotational particles (this is the friction type that is most frequently observed in dry granular media [8]), and that (2) we take rolling resistance as well as (3) convective and radiative effects into account. The first two of these features are of utmost importance to the modeling of systems that are supposed to attain a static equilibrium configuration after some given external excitation, which is the case for most types of problems we are interested here. The third feature, in turn, may be relevant if the temperatures to be experienced by the particles are sufficiently higher than the temperature of their surroundings, which may likewise occur in many applications. Another distinction is that our model makes use of contact and heat conduction parameters that are well grounded on physical models, in contrast to Zohdi's model, which adopts general parameters that,

although formally competent, require problem-dependent calibration for proper parameter values.

We highlight that our objective in this work is not to derive a complex, sophisticated model capable of furnishing extremely accurate results up to a very fine thermo-mechanical resolution, but instead to develop a sufficiently simple (yet robust) computational framework that contains all essential ingredients of thermo-mechanical particle systems. We aim to enable a practical, direct simulation tool, with which engineers and analysts may assess the overall system's response upon given (thermo-mechanical) external excitations, detecting general trends, identifying the relevance of certain parameters (and their subsequent impact upon the system's behavior), drawing what-if scenarios and thereby reliably improving process performance. For an early history of the discrete element method and reviews on its various applications, including major findings and fundamental results, we refer the reader to Bicanic [9], Zhu et al. [10, 11], O'Sullivan [12], Thornton et al. [13] and Radjai and Dubois [2], to cite just a few. For an overview of the modeling of dry particulate media and advanced manufacturing techniques, including both theoretical and practical aspects, we refer to Duran [8], Radjaï et al. [14], Zohdi [15] and Gibson et al. [16]. We believe that simple, consistent particle models of the type as shown here may be a useful tool to the modeling of discrete particle systems that are consisted of thermo-mechanically active particles and, in a broader sense, many other discrete systems wherein multiphysical effects may be relevant.

The text is organized as follows. In Sect. 2, we briefly describe our DEM formulation, with the various force and moment contributions that govern the particles' dynamics and their corresponding equations of motion. In Sect. 3, we present our model to incorporate thermal effects into the system's description, including detailed accounts of each possible heat transfer mechanisms and the influence of thermal softening on mechanical properties. In Sect. 4, we introduce our numerical method for solution of the system's equations, leading to a multiphysics (thermo-mechanical) staggered solution strategy embedded within an explicit time integration scheme (we also include an algorithmic overview and brief comments on implementational aspects). In Sect. 5, we show numerical examples to validate our model and illustrate its applicability, and in Sect. 6 we close the paper with our conclusions and final considerations. Throughout the text, plain italic letters ($a, b, \dots, \alpha, \beta, \dots, A, B, \dots$) denote scalar quantities, whereas boldface italic letters ($\boldsymbol{a}, \boldsymbol{b}, \dots, \boldsymbol{\alpha}, \boldsymbol{\beta}, \dots, \boldsymbol{A}, \boldsymbol{B}, \dots$) denote vectors in a three-dimensional Euclidean space. The (standard) inner product of two vectors is denoted by $\boldsymbol{u} \cdot \boldsymbol{v}$, and the norm of a vector by $\|\boldsymbol{u}\| = \sqrt{\boldsymbol{u} \cdot \boldsymbol{u}}$. Notation with a superposed dot is adopted to designate time derivatives.

2 Particles' dynamics

We follow a Lagrangian, discrete element description and consider, for the sake of simplicity (but without any loss of generality), only spherical particles here. Let us assume a system of N_P particles, each with mass m_i, radius r_i and rotational inertia (relative to the particle's center) $j_i = (2/5)m_i r_i^2$, $i = 1, \ldots, N_P$. We denote the position vector of a particle by x_i, the velocity vector by v_i, the incremental rotation vector by α_i^Δ (this is the rotation vector relative to two consecutive configurations) and the spin vector by ω_i. Following classical (Newton–Euler) dynamics, the equations of motion for the ith particle are

$$m_i \dot{v}_i = m_i g + f_i^{con} + f_i^{fric},$$
$$j_i \dot{\omega}_i = m_i^{fric} + m_i^{rol}, \tag{1}$$

where g is the gravity acceleration vector, f_i^{con} are the forces due to mechanical contacts (or collisions) with other particles and objects, f_i^{fric} are the forces due to friction (which arise from these contacts or collisions), m_i^{fric} is the moment due to the friction forces (these forces are eccentric w.r.t. the particle's center, and thereby generate a moment on the particle), and m_i^{rol} is the moment induced by rolling resistance effects (w.r.t. the particle's center). Each one of these force and moment contributions is briefly described next.

The contact forces are given as a function of the amount of overlap between any two contacting particles (or particle and object). We follow Hertz contact theory (see Johnson [17]) and adopt the following expression:

$$f_i^{con} = \sum_{j=1}^{N_i^c} f_{ij}^{con}, \quad \text{with} \quad f_{ij}^{con} = -\frac{4}{3}\sqrt{r^*}E^*\delta_{ij}^{3/2}n_{ij} - d^{con}\dot{\delta}_{ij}n_{ij}, \tag{2}$$

where f_{ij}^{con} is the force that acts on particle i due to its contact with particle (or object) j, N_i^c is the number of particles and objects that are in contact with particle i,

$$r^* = \frac{r_i r_j}{r_i + r_j} \quad \text{and} \quad E^* = \frac{E_i E_j}{E_j(1 - v_i^2) + E_i(1 - v_j^2)} \tag{3}$$

are the effective radius and the effective elasticity modulus of the i–j contacting pair (in which E_i, E_j, v_i and v_j are the elasticity modulus and the Poisson coefficient of i and j,

respectively), and δ_{ij} is the overlap between the pair, which is given by

$$\delta_{ij} = r_i + r_j - \left\| x_i - x_j \right\|. \tag{4}$$

Still in Eq. (2), n_{ij} is the contact normal direction, or unit vector that points from the center of particle i to the center of particle (or object) j, i.e.,

$$n_{ij} = \frac{x_j - x_i}{\left\| x_j - x_i \right\|}, \tag{5}$$

whereas d^{con} is the contact's damping constant (related to viscous energy dissipation in the normal direction), given by

$$d^{con} = 2\xi^{con}\sqrt{2E^*m^*\sqrt{r^*}}\,\delta_{ij}^{1/4}, \quad \text{with} \quad m^* = \frac{m_i m_j}{m_i + m_j}, \tag{6}$$

and $\dot{\delta}_{ij}$ is the overlap velocity of the contacting pair (i.e., relative velocity of the pair in the pair's central direction). In (6), ξ^{con} is the damping rate of the contact, which must be given (typically, one has $0 \leq \xi^{con} \leq 1$, with $\xi^{con} = 0$ standing for a perfectly elastic contact and $\xi^{con} = 1$ for a critically damped one).

The friction forces are given by Mindlin's elastic solution for sticking contact between spheres, combined with Coulomb's law for coupling the tangential force with the normal force whenever there is sliding (i.e., dynamic friction). Accordingly, denoting by f_{ij}^{fric} the force that acts on particle i due to its friction with particle (or object) j, for each contacting pair we first consider an elastic "trial stick state" in which the friction force is

$$f_i^{fric} = \sum_{j=1}^{N_i^c} f_{ij}^{fric,trial}, \quad \text{with} \quad f_{ij}^{fric,trial}$$
$$= -8G^*\sqrt{r^*}\delta_{ij}^{1/2}\Delta x_{ij}^{trial} - d^{fric}v_{ij,t}, \tag{7}$$

and then we verify it by a slip check against the static friction limit:

$$\begin{cases} \text{IF} \ \left\| f_{ij}^{fric,trial} \right\| \leq \mu_s \left\| f_{ij}^{con} \right\| \Rightarrow f_{ij}^{fric} = f_{ij}^{fric,trial} \ (\text{trial state is valid, sticking occurs between } i{-}j); \\ \text{IF} \ \left\| f_{ij}^{fric,trial} \right\| > \mu_s \left\| f_{ij}^{con} \right\| \Rightarrow f_{ij}^{fric} = \mu_d \left\| f_{ij}^{con} \right\| t_{ij} \ (\text{trial is not valid, sliding occurs between } i{-}j). \end{cases} \tag{8}$$

In Eq. (7), G^* is the effective shear modulus of the contacting pair, which is a function of the pair's individual shear moduli G_i and G_j as follows

$$G^* = \frac{G_i G_j}{G_i + G_j}, \tag{9}$$

and $\Delta \boldsymbol{x}_{ij}^{\text{trial}}$ is the pair's trial elastic deformation (total) in the tangential direction, which is computed incrementally through

$$\Delta \boldsymbol{x}_{ij}^{\text{trial}} = \Delta \boldsymbol{x}_{ij}^{\text{accum}} + \delta \boldsymbol{x}_{ij}^{\text{trial}}, \tag{10}$$

wherein $\Delta \boldsymbol{x}_{ij}^{\text{accum}}$ is the pair's accumulated deformation up to the previous configuration (i.e., the total deformation experienced by the pair until then, which must be known) and $\delta \boldsymbol{x}_{ij}^{\text{trial}}$ is the trial incremental deformation for the pair from the previous to the current configuration, whose expression is shown shortly below. Still in (7), d^{fric} is the friction damping constant, given by

$$d^{\text{fric}} = 2\xi^{\text{fric}} \sqrt{8G^* m^* \sqrt{r^*} \delta_{ij}^{1/4}} \tag{11}$$

(where ξ^{fric} is the frictional damping rate, which must be given) and $\boldsymbol{v}_{ij,t}$ is the tangential relative velocity between the contact points of i and j, respectively. In (8), in turn, μ_{s} and μ_{d} are the static and dynamic friction coefficients, whereas $\boldsymbol{t}_{ij} = \boldsymbol{v}_{ij,t} \left\| \boldsymbol{v}_{ij,t} \right\|^{-1}$ is the tangential (or sliding) direction of the pair. The pair's trial incremental deformation is computed through time integration of the tangential relative velocity between the contact points of i and j from the previous to the current configuration, i.e.,

$$\delta \boldsymbol{x}_{ij}^{\text{trial}} = \int_{t}^{t+\Delta t} \boldsymbol{v}_{ij,t}(\tau)\mathrm{d}\tau, \tag{12}$$

where t is the time instant of the previous configuration and $t + \Delta t$ that of current. In case of sliding, since the sticking assumption is violated, the total deformation in the tangential direction is not the trial deformation, but may be computed from this later through a return (or correction) scheme, from which one has

$$\Delta \boldsymbol{x}_{ij} = \frac{1}{8G^* \sqrt{r^*} \delta_{ij}^{1/2}} \left(\mu_{\text{d}} \left\| \boldsymbol{f}_{ij}^{\text{con}} \right\| \boldsymbol{t}_{ij} - d^{\text{fric}} \boldsymbol{v}_{ij,t} \right). \tag{13}$$

We remark that the total deformation of every contacting pair must be stored after the above computations, as to become available for evaluation of the pairs' friction forces in the next configuration. This is accomplished through setting $\Delta \boldsymbol{x}_{ij}^{\text{accum}} \leftarrow \Delta \boldsymbol{x}_{ij}^{\text{trial}}$ (if the trial state was valid) or else through $\Delta \boldsymbol{x}_{ij}^{\text{accum}} \leftarrow \Delta \boldsymbol{x}_{ij}$ (if sliding occurred). For a detailed algorithmic treatment, we refer the reader to Campello [3].

The moments due to the friction forces (relatively to the center of the particle) are given by

$$\boldsymbol{m}_{i}^{\text{fric}} = \sum_{j=1}^{N_i^c} \boldsymbol{m}_{ij}^{\text{fric}}, \quad \text{with} \quad \boldsymbol{m}_{ij}^{\text{fric}} = \sum_{j=1}^{N_i^c} \boldsymbol{r}_{ij} \times \boldsymbol{f}_{ij}^{\text{fric}}, \tag{14}$$

where $\boldsymbol{m}_{ij}^{\text{fric}}$ is the moment on particle i due to its friction with particle (or object) j, and $\boldsymbol{r}_{ij} = r_i \boldsymbol{n}_{ij}$ is the vector that connects the center of particle i to its contact point with particle j.

The moments due to rolling resistance, in turn, are given by a rotational spring-damper-slider model (often also called an "elastic–plastic" model), which may be thought of as the rotational version of the stick–slip friction model presented above. Accordingly, denoting by $\boldsymbol{m}_{ij}^{\text{rol}}$ the moment that acts on particle i due to its rolling over particle (or object) j, for each rolling pair we first consider an elastic trial stick state in which the rolling resistance moment is

$$\boldsymbol{m}_{i}^{\text{rol}} = \sum_{j=1}^{N_i^c} \boldsymbol{m}_{ij}^{\text{rol,trial}}, \quad \text{with} \quad \boldsymbol{m}_{ij}^{\text{rol,trial}}$$
$$= -8G^* \sqrt{r^*} \delta_{ij}^{1/2} (r^*)^2 \Delta \boldsymbol{\theta}_{ij}^{\text{trial}} - d^{\text{rol}} \boldsymbol{\omega}_{ij}, \tag{15}$$

and then we verify it by a slip check against the static rolling (or "yield") limit:

$$\begin{cases} IF \quad \left\| \boldsymbol{m}_{ij}^{\text{rol,trial}} \right\| \leq \mu_{\text{r}} r^* \left\| \boldsymbol{f}_{ij}^{\text{con}} \right\| \Rightarrow \boldsymbol{m}_{ij}^{\text{rol}} = \boldsymbol{m}_{ij}^{\text{rol,trial}} \ (\text{trial state is valid, sticking occurs}); \\ IF \quad \left\| \boldsymbol{m}_{ij}^{\text{rol,trial}} \right\| > \mu_{\text{r}} r^* \left\| \boldsymbol{f}_{ij}^{\text{con}} \right\| \Rightarrow \boldsymbol{m}_{ij}^{\text{rol}} = \mu_{\text{r}} r^* \left\| \boldsymbol{f}_{ij}^{\text{con}} \right\| \boldsymbol{s}_{ij} \ (\text{trial is not valid, sliding occurs}). \end{cases} \tag{16}$$

In Eq. (15), $\Delta \boldsymbol{\theta}_{ij}^{\text{trial}}$ is the pair's trial rolling rotation (total), which is computed incrementally through

$$\Delta \boldsymbol{\theta}_{ij}^{\text{trial}} = \Delta \boldsymbol{\theta}_{ij}^{\text{accum}} + \delta \boldsymbol{\theta}_{ij}^{\text{trial}}, \tag{17}$$

where $\Delta \boldsymbol{\theta}_{ij}^{\text{accum}}$ is the pair's accumulated rolling rotation up to the previous configuration (i.e., the total rolling rotation experienced by the pair until then, which must be known) and $\delta \boldsymbol{\theta}_{ij}^{\text{trial}}$ is the trial incremental rolling rotation for the pair from the previous to the current configuration, whose expression is shown shortly below. Still in (15), d^{rol} is the rolling damping constant, given by

$$d^{\text{rol}} = 2\xi^{\text{rol}} \sqrt{8G^* j^* \sqrt{r^*} r^* \delta_{ij}^{1/4}},$$
$$\text{with} \quad j^* = \left(\frac{1}{j_i + m_i r_i^2} + \frac{1}{j_j + m_j r_j^2} \right)^{-1}, \tag{18}$$

(where ξ^{rol} is the rolling damping rate, which must be given), and $\boldsymbol{\omega}_{ij} = \boldsymbol{\omega}_i - \boldsymbol{\omega}_j$ is the relative rolling velocity between the pair. In (16), in turn, μ_{r} is the rolling resistance coefficient,

whereas $s_{ij} = \boldsymbol{\omega}_{ij} \left\| \boldsymbol{\omega}_{ij} \right\|^{-1}$ is the sliding rolling axis of the pair. The pair's trial incremental rolling rotation is computed through time integration of the relative rolling velocity between i and j from the previous to the current configuration, i.e.,

$$\delta \boldsymbol{\theta}_{ij}^{\text{trial}} = \int_{t}^{t+\Delta t} \boldsymbol{\omega}_{ij}(\tau) \mathrm{d}\tau. \tag{19}$$

In case of sliding, since the sticking assumption is violated, the total rolling rotation is not the trial rolling rotation, but may be computed from this later through a return scheme, from which one has

$$\Delta \boldsymbol{\theta}_{ij} = \frac{1}{8G^* \sqrt{r^*} \delta_{ij}^{1/2} (r^*)^2} \left(\mu_r r^* \left\| \boldsymbol{f}_{ij}^{\text{con}} \right\| s_{ij} - d^{\text{rol}} \boldsymbol{\omega}_{ij} \right). \tag{20}$$

We remark that, similarly as to the friction force model, the total rolling rotation of every rolling pair must be stored after the above computations, as to become available for evaluation of the pairs' rolling resistance moments in the next configuration. This is accomplished through setting $\Delta \boldsymbol{\theta}_{ij}^{\text{accum}} \leftarrow \Delta \boldsymbol{\theta}_{ij}^{\text{trial}}$ (if the trial state was valid) or else through $\Delta \boldsymbol{\theta}_{ij}^{\text{accum}} \leftarrow \Delta \boldsymbol{\theta}_{ij}$ (if sliding occurred). Again, for a detailed algorithmic treatment, we refer the reader to Campello [3].

Remark 1 The consideration of other force and moment contributions, such as adhesion forces, near-field interactions, electromagnetic effects from external fields, drag forces (from the surrounding environment), van der Waals effects, as well as other rolling resistance models, is entirely possible, but not considered here. The interested reader is referred to Campello [3, 5] and Campello and Zohdi [18] for details. Also, it is worth mentioning that the interaction between particles and rigid walls may be represented as a special case of that between particles, simply by taking the walls with infinite mass, radius, inertia and elastic parameters in the above force and moment expressions.

Remark 2 Some of the particles' mechanical properties, such as the elasticity modulus, may vary with temperature, providing some sort of thermal softening (or stiffening) due to a change in temperature. This is one source of coupling between the thermal and mechanical fields and can be taken into account in a straightforward way by simply considering a temperature-dependent value for the corresponding property (e.g., from a given input curve), instead of a constant-valued one. This will be dealt with in Sect. 3.5. Another source of coupling is the heat transfer between particles through conduction, which is dependent on the particles' contact area and the distance between their centers—and thereby, on the particles' positions and velocities, as will be seen in Sect. 3.2.

3 Consideration of thermal effects

Following the same discrete particle approach as for the mechanical fields, we assume here that the temperatures are uniform within the particles. This corresponds to a lumped thermal model and is valid as long as the particles are relatively small, such that their surface area is large enough in relation to their interior volume as to allow for a rapid exchange of heat with the surrounding medium—which is the case here.[1] From the first law of thermodynamics, the energy balance for the ith particle reads

$$\dot{K}_i + \dot{U}_i^{\text{int}} = P_i^{\text{ext}} + \dot{Q}_i^{\text{ext}} + \dot{Q}_i^{\text{cond}} + \dot{Q}_i^{\text{conv}} + \dot{Q}_i^{\text{rad}}, \tag{21}$$

where K_i is the particle's kinetic energy, U_i^{int} is the particle's internal (or stored) (mechanical plus thermal) energy, P_i^{ext} is the mechanical power due to the external forces, Q_i^{ext} is the particle's heat input from external devices (e.g., fire nozzles, burners, laser beams, electric currents, etc.), Q_i^{cond} is the particle's heat flow due to conduction (amount of heat that flows through the particle by conduction upon contact with other particles and objects), Q_i^{conv} is the particle's heat flow due to convection by its surroundings (amount of heat that flows from or to the particle due to convection by the surrounding environment) and Q_i^{rad} is the particle's heat flow due to radiative effects. The kinetic energy is given by

$$K_i = \frac{1}{2} m_i \boldsymbol{v}_i \cdot \boldsymbol{v}_i, \tag{22}$$

with its time derivative being

$$\dot{K}_i = m_i \dot{\boldsymbol{v}}_i \cdot \boldsymbol{v}_i. \tag{23}$$

Consistent with the DEM assumptions, the particle's deformations (due to contacts with other particles and objects) are assumed to be very small, such that the mechanical part of the internal or stored energy is negligible. There remains only its thermal part, which means that

$$U_i^{\text{int}} = m_i C_i \theta_i, \tag{24}$$

where C_i is the specific heat of the particle (heat capacity per unit mass, which is assumed constant) and θ_i is the particle's temperature. The time derivative of (24) yields

$$\dot{U}_i^{\text{int}} = m_i C_i \dot{\theta}_i. \tag{25}$$

---

[1] A useful measure to ascertain such an assumption is the Biot number, which must be small (smaller than one). The Biot number for spheres scales with the ratio of the sphere's volume to the sphere's surface area, i.e., with the sphere's radius. Since the particles are assumed to be small here, of the order of micrometers to a few millimeters, the Biot number will always be small (much smaller than one).

The power due to the external forces is

$$P_i^{\text{ext}} = f_i^{\text{tot}} \cdot v_i, \tag{26}$$

where f_i^{tot} is the total force vector acting on the particle, which is the sum of all forces on the right-hand side of Eq. (1)$_1$. From the balance of linear momentum on the particle, one has $m_i \dot{v}_i = f_i^{\text{tot}}$, and if this is inserted into Eq. (23) it follows that

$$\dot{K}_i = P_i^{\text{ext}}, \tag{27}$$

implying that these two terms cancel out each other in Eq. (21). As a consequence, and taking (25) into account, the energy balance of the particle reads

$$m_i C_i \dot{\theta}_i = \dot{Q}_i^{\text{ext}} + \dot{Q}_i^{\text{cond}} + \dot{Q}_i^{\text{conv}} + \dot{Q}_i^{\text{rad}}. \tag{28}$$

This expression is formally identical to Eq. (1), except that it is now a scalar equation. It is the governing equation for the system's thermal field. Each one of its heat power (or heat flow per unit time) contributions is described in the subsections that follow.

3.1 Heat power due to external devices

The heat power provided by external devices (fire nozzles, burners, laser beams, electric currents, etc.) can be described through given (ad-hoc) expressions according to the type of device that is heating up the system. A general expression is

$$\dot{Q}_i^{\text{ext}} = a_i I_i^{\text{dev}}, \tag{29}$$

where $0 \leq a_i \leq 1$ is the particle's absorptance (or absorptivity, ratio of the absorbed to the incident heat power, ascertaining the effectiveness of the particle's surface in absorbing heat), which must be known, and I_i^{dev} is the device's input power at the particle's location, which must also be known. For, e.g., fire nozzles, one possible expression for I_i^{dev} is

$$I_i^{\text{dev}} = I_0 A_i \left(1 - \frac{z_i}{d_{\max}} \right), \tag{30}$$

where I_0 is the nozzle's nominal input intensity (power per unit area of the nozzle's cross section, which must be known), $A_i = \pi r_i^2$ is the particle's frontal area (i.e., the area that is exposed to the nozzle's power), $d_{\max}$ is the maximum penetration (or heating reach) of the nozzle within the bulk of the material (which must also be known) and $0 \leq z_i \leq d_{\max}$ is the particle's depth with respect to the nozzle's striking position (measured along the nozzle's path-length, as indicated in Fig. 1). This is based on the assumption that the nozzle's power attenuates linearly inside the material until the maximum depth $d_{\max}$ is reached. If, e.g.,
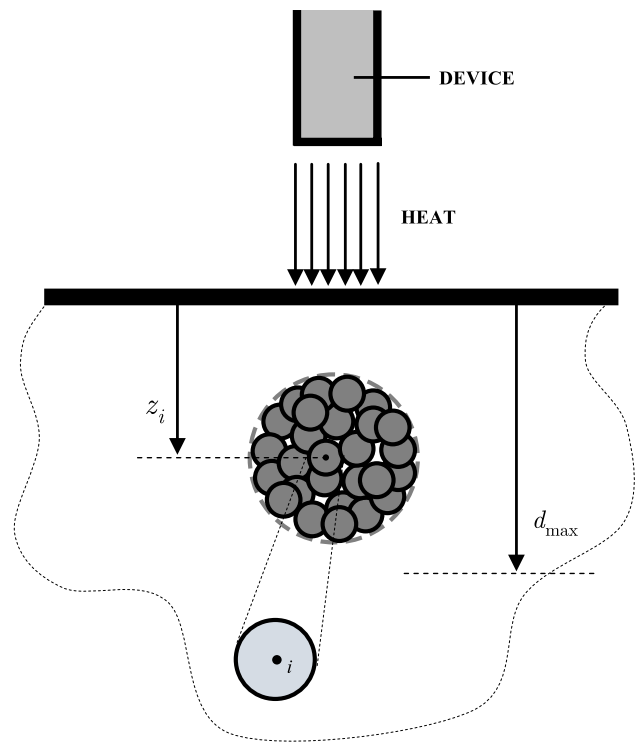

Fig. 1 Representation of external device's heat penetration within a granular material. The depth of a particle w.r.t. the device's striking position is measured by z_i, whereas the device's maximum penetration (or heating reach) is $d_{\max}$

the nozzle is such that its power affects only the surface of the material, not penetrating its interior, one must set $d_{\max} = r_i^{\text{top}}$, with r_i^{top} as the radius of the top-layer particles, implying that only these particles will be directly heated by the nozzle (all sub-surface heating will be accomplished by conduction from the top layer). For laser beams, in turn, one possible expression for I_i^{dev} may be derived from the Lambert–Beer law, which states that the attenuation of incident light through a material (by both absorption and scattering) is exponentially dependent on the material's thickness (or, more precisely, optical depth) and its attenuation coefficient. Accordingly, we write

$$I_i^{\text{dev}} = I_0 A_i e^{-\mu z_i}, \tag{31}$$

where I_0 is the laser's input intensity (power per unit area of the beam's cross section, which must be known), $A_i = \pi r_i^2$ is the particle's frontal area, μ is the material's attenuation coefficient (a bulk property determining how much the radiant power of the beam is reduced as it passes through the bulk of the material, with units of m^{-1}) and z_i is the particle's depth w.r.t. the beam's striking position (measured along the beam's path-length, as indicated in Fig. 1). This expression is obtained by assuming uniform attenuation in the Lambert–Beer law, in the sense that μ does not vary throughout
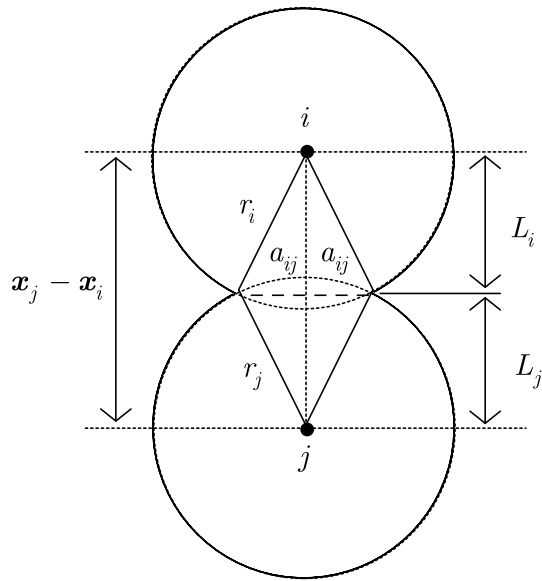
Fig. 2 Geometrical representation of two contacting particles allowing for the solution to obtain L_i

the path-length of the beam. We remark that consideration of the transmittance of the laser through the interior of the material is of utmost importance. Otherwise, only the surface layer remains hit by the beam, leaving all deeper (subsurface) heating to be accomplished solely by conduction from the top layer—a scenario that is far too conservative for laser devices. Considering the penetration of the heat source through the bulk of the material allows the deeper parts to be heated up more rapidly and effectively and represents the physical process in a more reliable way. Other expressions for the device's input power may be adopted, according to the problem at hand.

3.2 Heat power due to conduction

Heat flow through conduction takes place whenever the particle makes contact with another particle or object. It is a function of the temperature gradient between the contacting pair, the contact area between the pair and the pair's individual thermal conductivities. We follow the discrete form of Fourier's law for conduction across interfaces and adopt the following expression

$$\dot{Q}_i^{\mathrm{cond}} = \sum_{j=1}^{N_i^c} \dot{Q}_{ij}^{\mathrm{cond}}, \quad \text{with} \quad \dot{Q}_{ij}^{\mathrm{cond}} = k_{ij} \frac{\theta_j - \theta_i}{\left\| \boldsymbol{x}_j - \boldsymbol{x}_i \right\|} A_{ij}^c, \quad (32)$$

where Q_{ij}^{cond} is the conduction heat flow on particle i due to its contact with particle (or object) j, N_i^c is the number of particles and objects that are in contact with particle i, k_{ij} is the effective thermal conductivity of the $i-j$ contacting pair (which is a function of the individual thermal conductivities of i and j and, possibly, the thermal resistance at their interface) and A_{ij}^c is the contact area between the pair. This latter is computed by assuming that the area is circular with radius a_{ij}, which in turn may be obtained through solution of the following geometrical problem (see Fig. 2):

$$
\begin{aligned}
a_{ij}^2 + L_i^2 &= r_i^2 \\
a_{ij}^2 + L_j^2 &= r_j^2 \\
L_i + L_j &= \left\| \boldsymbol{x}_j - \boldsymbol{x}_i \right\|,
\end{aligned}
\tag{33}
$$

which gives (see Zohdi [19])

$$L_i = \frac{1}{2}\left(\left\| \boldsymbol{x}_j - \boldsymbol{x}_i \right\| - \frac{r_j^2 - r_i^2}{\left\| \boldsymbol{x}_j - \boldsymbol{x}_i \right\|} \right) \quad \Rightarrow \quad A_{ij}^c = \pi a_{ij}^2 = \pi (r_i^2 - L_i^2). \tag{34}$$

We draw the attention of the reader to the fact that Hertz contact theory predicts $A_{ij}^c = \pi(r^* \delta_{ij})$ (with r^* and δ_{ij} given, respectively, by Eqs. (3)$_1$ and (4)), but this is valid only for very small overlaps. Expression (34), on the contrary, is general and holds for any overlap magnitude.

The pair's effective thermal conductivity may be computed from

$$\frac{r_i + r_j}{k_{ij}} = \frac{r_i}{k_i} + \frac{r_j}{k_j}, \tag{35}$$

where k_i and k_j are the thermal conductivities of i and j, respectively, and r_i and r_j their radii. If the particles have adsorbed material onto their surfaces, one extra term may be added to the above expression to account for the corresponding thermal resistance (namely, the term would be $t_{\mathrm{mat}}/k_{\mathrm{mat}}$, where t_{mat} is the material's thickness and k_{mat} its thermal conductivity). Expression (35) is based on the assumption that the individual thermal resistances of the contacting pair may be summed up to provide the effective resistance of the pair, the reciprocal of which furnishes the pair's effective conductivity.

An alternative approach, though valid only for 2D particles (i.e., circles or disks), is to consider the so-called pipe network model from Feng et al. [20], which is based on the thermal conductances of the contacting particles (rather than on their thermal conductivities) and the formation of a "heat pipe" between the contacting pair at their contact interface. Accordingly, if α_i is the angle (measured from the particle's center) that defines the particle's contact interface

with another particle or object, the thermal conductance κ_i of the particle may be satisfactorily approximated by

$$\kappa_i \cong \frac{\pi k_i}{-\ln \alpha_i + 3/2 + \alpha_i^2/36 + \alpha_i^4/2700} \; . \tag{36}$$

This result is based on the two-dimensional solution of the steady-state heat problem within a 2D circular domain to which heat is provided across an interface defined by α_i. A similar expression holds for the thermal conductance of particle j. The effective conductance of the contacting pair is then obtained as the reciprocal of the effective resistance, similarly to (35). The three-dimensional version of this model is yet to appear. Other possible approaches, also based on conductances rather than on conductivities, are as suggested by Radjai and Dubois [2] and Vargas-Escobar [1]. We remark that we prefer to work with the conductivity rather than with the conductance, since the former is a material property, whereas the latter is a component-based one. One additional possible approach is by combining a discrete-finite element representation for the particles and their interfaces, e.g., in Yan and Jiao [21] and Yan et al. [22], but this is clearly not within the scope of our work.

The thermal conductivities of the particles are assumed to be constant with temperature here (although we could easily consider temperature-varying ones, in the lines of what is done for the mechanical properties in Sect. 3.5). This is a reasonable approximation for a wide range of engineering materials and operating temperatures—at least as long as the particles do not approach or experience phase transformation, which is the case here. Note that expressions (32) and (34) stand for a source of coupling between the thermal and mechanical fields, as it had been previously mentioned in a remark at the bottom of Sect. 2.

3.3 Heat power due to convection

The surrounding environment (e.g., the environmental air) may exchange heat with the particle through convection. The corresponding heat flow on the particle may be computed through the classical Newton's law of cooling. We adopt the following expression

$$\dot{Q}_i^{\text{conv}} = h_i(\theta_{\text{E}} - \theta_i)A_i^s, \tag{37}$$

where h_i is the convection (or film) coefficient of the particle w.r.t its surrounding environment, θ_{E} is the environment's temperature at the particle's location (which must be known) and $A_i^s = 4\pi r_i^2$ is total surface area of the particle. We assume that the convection coefficient is independent (or only marginally dependent) of the temperature difference between the particle and the environment. By resorting to the Nusselt number Nu of the environment around the particle (ratio between its heat transfer of convection to heat

transfer of conduction), the convection coefficient may be given by

$$\text{Nu} = \frac{h_i L}{k_{\text{E}}} \quad \Rightarrow \quad h_i = \frac{\text{Nu}k_{\text{E}}}{L}, \tag{38}$$

where $L = 2r_i$ is the length scale and k_{E} is the environment's thermal conductivity. The Nusselt number may be related to the Reynolds number and Prandtl number through the well-known heat transfer expression for flows past single spheres (see Whitaker [23])

$$\text{Nu} \approx 2 + \left(0.4\text{Re}^{1/2} + 0.06\text{Re}^{2/3}\right)\text{Pr}^{0.4}\left(\frac{\mu_{\text{E}}}{\mu_{\text{E,s}}}\right)^{0.25}, \tag{39}$$

where

$$\text{Pr} = \frac{C_{\text{E}}\mu_{\text{E}}}{k_{\text{E}}} \tag{40}$$

is the Prandtl number (wherein C_{E} is the environment's specific heat), μ_{E} is the environment's fluid viscosity and $\mu_{\text{E,s}}$ its viscosity at the particle's surface temperature (we assume $\mu_{\text{E,s}} \approx \mu_{\text{E}}$ throughout this work). Expression (39) is a semi-empirical relation and allows for a realistic estimate to the convection coefficient of smooth spheres for a wide range of heat transfer and fluid flow regimes.[2] For nearly stationary particles within calm (stagnant) environments, as the Reynolds number tends to zero, and consequently the Nusselt number to two, from (38) one has $h_i \cong k_{\text{E}}/r_i$. This resembles natural (i.e., free) convection situations and will be adopted throughout this work (unless otherwise stated, where then Eq. (38) with (39) would hold). We remark that the above model is a "one-way" type of model, in the sense that the environment's temperature affects the particles but the particles' temperatures do not affect the environment. This may seem a rather rough approximation, but suffices for the purposes of this work (we recall that we are not interested in having extremely accurate results here, but instead in developing a simple model that covers the essential ingredients of thermo-mechanical particle systems and capture their overall behavior for practical applications; besides, this approximation is consistent with the small particles assumption). More elaborate approaches, e.g., solving for both the environment's and particle's temperatures in a large-scale CFD (computational fluid dynamics) coupled analyses, are obviously possible, but not considered here (this is clearly outside the scope of the present work).

---

[2] The effects of particle spin on the convection coefficient, and thereby on the overall convective cooling rates of the particles, are neglected here. This is arguable, and we leave it as matter of future research.
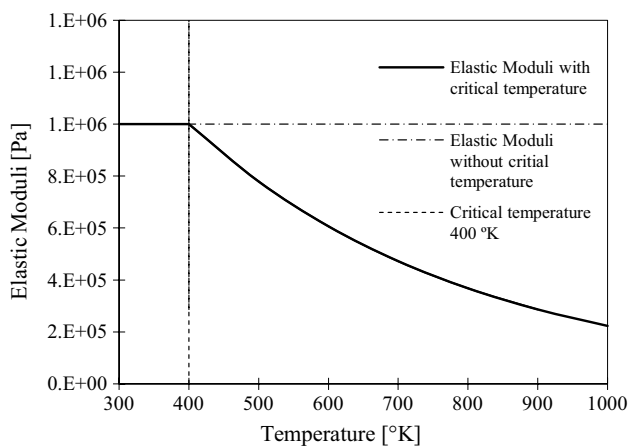
Fig. 3 Schematic illustration of the thermal degradation of a particle's elasticity modulus as implied by the proposed relation. Other mechanical properties may likewise vary with temperature, such as the friction coefficient and the adhesion stiffness, but this will not be considered here

3.4 Heat power due to radiation

Heat flow by radiative effects may be relevant if the particle's surrounding environment (e.g., the environmental air) has a significantly different temperature as compared to the particle's own temperature. In many applications, the particles are severely heated, whereas its surroundings remain (at least in an average sense) at a much lower temperature. In such condition, the amount of electromagnetic thermal radiation that is emitted by a particle may be significantly larger than that absorbed by it from the environment, creating an outward net energy flow from the particles that ultimately promotes overall cooling of the system. We follow the Stefan–Boltzmann law to account for this energy transfer mechanism and adopt the following expression:

$$\dot{Q}_i^{\mathrm{rad}} = \varepsilon_i B(\theta_{\mathrm{E}}^4 - \theta_i^4) A_i^s , \tag{41}$$

where $0 \leq \varepsilon_i \leq 1$ is the particle's radiative cooling efficiency (which must be known), $B = 5.670367 \times 10^{-8}$ W/m^2 K^4 is the Stefan–Boltzmann constant, θ_{E} is the environment's temperature at the particle's location (which must also be known) and $A_i^s = 4\pi r_i^2$ is the particle's surface area. Again, the environment's temperature, besides being known (i.e., given), is assumed to be unaffected by the particle's temperature (a "one-way" model). We once again acknowledge that this may be a rather rough approximation, but for the same reasons mentioned in the previous subsection it suffices for the purposes of this work (besides, it is also consistent with the small particles assumption).

3.5 Thermal softening of mechanical properties

Most materials have their mechanical properties degraded with increasing temperature. To incorporate such softening effects into the particles' dynamics, one straightforward way is to consider temperature-dependent mechanical properties (e.g., by means of given input curves), instead of constant-valued ones. Accordingly, we adopt the following expression for the particles' elasticity modulus:

$$E_i = \hat{E}_i(\theta_i) = \min\left\{ E_0, E_0 \mathrm{e}^{1 - \frac{\theta_i}{\theta^*}} \right\} , \tag{42}$$

where E_0 is the modulus' ground or reference value (e.g., the value at room temperature, or at a temperature interval around the room temperature) and θ^* is the critical temperature at which it starts to degrade. A threshold value $E_{\min}$ may also be introduced, as to prevent indefinite softening. Figure 3 depicts (qualitatively) the general behavior implied by this relation for a ground modulus of $E_0 = 1.0$ MPa and a critical temperature of $\theta^* = 400$ K. Expression (42) may also be modified as to include a degrading rate coefficient, which would multiply the temperature term on the exponent. This would allow one to fine-tune the strength or mildness of the decaying rate, and thereby approximate other softening behaviors such as linear and hyperbolic softening (as commonly observed for many metals and ceramic materials). One should notice that thermal softening affects not only the particle's normal stiffness (and therefrom its normal contact forces), but also its tangential stiffness (and thus its friction forces and rolling resistance moments), since the elasticity modulus enters the expression of the particle's shear modulus. The thermal softening of many common engineering materials may be satisfactorily approximated by expression (42). Other ad-hoc relations (e.g., multilinear or more elaborate laws) are likewise possible to be incorporated.

Remark 3 The consideration of other heat sources and energy transfer mechanisms, such as heating or cooling due to internal chemical reactions (triggered, e.g., by reactive thin films adsorbed onto the particles' surface, which may be activated by inter-particle collisions), is entirely possible, but not considered here. The onset and subsequent progress of such reactions may be represented through simple evolution laws that capture their overall influence on the mechanical and thermal states of the particles. Also, heat dissipated through inelastic impacts, as well as induced by dragging effects (due to friction with the surrounding environment at high speeds), are likewise possible, but will not be considered here (for a straightforward way to deal with drag-induced heating, see e.g., Campello [24]). These advancements are being currently undertaken by the authors and shall appear soon in a forthcoming paper.

4 Numerical solution scheme

To compute the time evolution of the system, we integrate the governing Eqs. (1) and (28) numerically by means of an explicit (forward Euler) scheme. Accordingly, for the velocities and spins of the particles, between any two time instants t and $t + \Delta t$ we have

$$\theta_i(t + \Delta t) = \theta_i(t) + \frac{1}{m_i C_i} \int_t^{t+\Delta t} (\dot{Q}_i^{\text{ext}} + \dot{Q}_i^{\text{cond}} + \dot{Q}_i^{\text{conv}} + \dot{Q}_i^{\text{rad}}) dt$$
$$\approx \theta_i(t) + \frac{\Delta t}{m_i C_i} \left(\dot{Q}_i^{\text{ext}}(t) + \dot{Q}_i^{\text{cond}}(t) + \dot{Q}_i^{\text{conv}}(t) + \dot{Q}_i^{\text{rad}}(t) \right) . \quad (46)$$

The solution process is very straightforward, as schematically outlined in the algorithm below:

---

1. Initialize time variables and get initial conditions:
   $t = 0$, $\Delta t =$ given
   $\boldsymbol{x}_i(0),\ \boldsymbol{v}_i(0),\ \boldsymbol{\omega}_i(0),\ \boldsymbol{\alpha}_i(0),\ \theta_i(0) =$ given.
2. Compute forces and moments at time t via equations (2), (7)–(8), (14) and (15)–(16), taking (42) into account.
3. Compute heat powers at time t via equations (29), (32), (37) and (41).
4. Freeze thermal field and update velocities, spins, positions and incremental rotations via equations (43) and (44).
5. Freeze mechanical fields and update temperatures through equation (46).
6. Save updated variables and move to next time step:
   $\boldsymbol{v}_i(t) \leftarrow \boldsymbol{v}_i(t + \Delta t),$
   $\boldsymbol{\omega}_i(t) \leftarrow \boldsymbol{\omega}_i(t + \Delta t),$
   $\boldsymbol{x}_i(t) \leftarrow \boldsymbol{x}_i(t + \Delta t),$
   $\boldsymbol{\alpha}_i(t) \leftarrow \boldsymbol{\alpha}_i(t + \Delta t),$
   $\theta_i(t) \leftarrow \theta_i(t + \Delta t),$
   $t \leftarrow t + \Delta t$
   Go to step 2.

$$\boldsymbol{v}_i(t + \Delta t) = \boldsymbol{v}_i(t) + \frac{1}{m_i} \int_t^{t+\Delta t} (m_i \boldsymbol{g} + \boldsymbol{f}_i^{\text{con}} + \boldsymbol{f}_i^{\text{fric}}) dt$$
$$\approx \boldsymbol{v}_i(t) + \frac{\Delta t}{m_i} \left(m_i \boldsymbol{g} + \boldsymbol{f}_i^{\text{con}}(t) + \boldsymbol{f}_i^{\text{fric}}(t) \right) ,$$
$$\boldsymbol{\omega}_i(t + \Delta t) = \boldsymbol{\omega}_i(t) + \frac{1}{j_i} \int_t^{t+\Delta t} (\boldsymbol{m}_i^{\text{fric}} + \boldsymbol{m}_i^{\text{rol}}) dt$$
$$\approx \boldsymbol{\omega}_i(t) + \frac{\Delta t}{j_i} \left(\boldsymbol{m}_i^{\text{fric}}(t) + \boldsymbol{m}_i^{\text{rol}}(t) \right) , \quad (43)$$

where Δt is the integration time-step size, whereas for the positions and incremental rotations we write

$$\boldsymbol{x}_i(t + \Delta t) \approx \boldsymbol{x}_i(t) + \boldsymbol{v}_i(t + \Delta t)\Delta t ,$$
$$\boldsymbol{\alpha}_i^{\Delta}(t + \Delta t) \approx \boldsymbol{\omega}_i(t + \Delta t)\Delta t . \quad (44)$$

The total rotation vectors are obtained by means of the Rodrigues formula (see Campello [4])

$$\boldsymbol{\alpha}_i(t + \Delta t) = \frac{4}{4 - \boldsymbol{\alpha}_i(t) \cdot \boldsymbol{\alpha}_i^{\Delta}(t + \Delta t)}$$
$$\left(\boldsymbol{\alpha}_i(t) + \boldsymbol{\alpha}_i^{\Delta}(t + \Delta t) - \frac{1}{2} \boldsymbol{\alpha}_i(t) \times \boldsymbol{\alpha}_i^{\Delta}(t + \Delta t) \right) . \quad (45)$$

For the thermal states of the particles, in turn, we have

Since we adopt an explicit scheme, selection of an appropriate time-step size for a numerically stable time integration is critical. As general guideline, Δt must be set as a fraction of the smaller vibration period of all particle interactions (forces, moments and heat transfer contributions) of the model. Here, however, since we are dealing with problems wherein contacts and collisions inherently occur, and since they are typically of very short duration, the time-step size is invariably governed by the duration of the contacts—at least for the types of problems we are interested in and the material properties we consider. Thus, we adopt the following criterion:

$$\Delta t \le \frac{\delta t_{\text{con}}}{10} , \quad \delta t_{\text{con}} \cong 2.87 \left[\frac{(m^*)^2}{r^* (E^*)^2 v_{\text{rel}}} \right]^{1/5} , \quad (47)$$

where δt_{con} is the duration of the shortest possible contact or collision of the system and v_{rel} is the relative velocity of the corresponding contacting pair in the pair's central direction immediately before the contact or collision is initiated. This is based on Hertz's contact theory (see Johnson [17]) and, according to our experience, allows for a good accuracy in the computation of the contact forces.

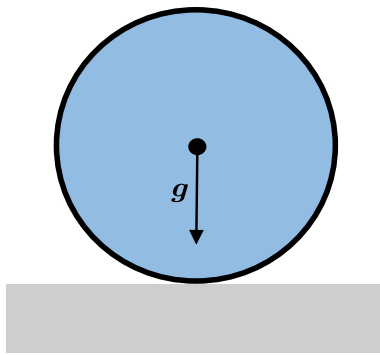One additional important aspect is that contact detection is often the computational bottleneck of any DEM solution

Fig. 4 Single particle under gravity placed over a thermally active floor

scheme. We perform this task here via a hybrid global–local search method, wherein both domain subdivision cells and nearest-neighbors lists ("Verlet lists") are combined. Details on its algorithmic implementation can be found in Campello [5].

Remark 4 The use of implicit time integration schemes, such as the backward Euler scheme or the midpoint rule, is entirely possible within this framework (see, e.g., Campello [3] and Zohdi [6]). Here, however, since we are interested in having a "first working version" of the model in its simplest form, and since we are not concerned with long-term calculations (for which accuracy could be an issue), explicit, first-order accurate methods are sufficient. The implicit version is currently under development by the authors, using a recursive (fixed-point iterative) error-controlled approach within each time step.

5 Numerical examples

Let us illustrate the usage of the above model by analyzing a few numerical examples. First, we show one simple validation problem involving only a single particle (we remark that extensive validation of the model has been conducted in a separate study and will not be reported here). Next, we analyze more general, multi-particle model problems.

5.1 Interaction between a particle and a thermal base

This example is analyzed to investigate the behavior of the basic ingredient of a thermo-mechanical particle system, namely the interaction between two contacting entities. For simplicity, we consider here a single particle in contact with a thermal floor, with arbitrarily different initial temperatures. We want to assess some of the features of our scheme under simple idealized conditions, such that we may

better highlight its coupled thermal–mechanical aspects. In particular, we want to evaluate the evolution of the particle's temperature and its subsequent effect upon the particle's elastic stiffness and contact force. Let us consider a particle with radius $r_1 = 0.001$ m, placed tangentially over a thermally active base, as shown in Fig. 4. Gravity acts downwards. The particle has an initial temperature $\theta_1(0) = 300$ K and is made of a material with thermal conductivity $k_1 = 60$ W/m K, specific heat $C_1 = 100$ J/kg K, mass-density $\rho_1 = 3000$ kg/m^3 and elastic properties at room temperature $E_{0,1} = 1.0$ MPa and $\nu_1 = 0.3$, with critical (degrading) temperature $\theta_1^* = 400$ K. Critically damped contact is considered ($\xi^{con} = 1$). The floor is assumed to have infinite mass and zero conductivity (i.e., it does not change its thermal state over time), with a constant temperature of $\theta_f = 700$ K. The surrounding environment is not considered (i.e., it does not absorb nor provide heat to the particle). As gravity drives the particle toward the floor, they make contact and the particle starts to receive heat through conduction, since it is at a smaller temperature than the floor. Eventually, the particle attains mechanical and thermal equilibrium with the floor. Figure 5 depicts the evolution of the particle's temperature with time, along with time histories of its elastic moduli, overlap, contact area and contact force. As we can see in Fig. 5a, thermal equilibrium is reached at around $t \approx 12$ s. The elastic moduli is clearly seen to degrade (Fig. 5b), and the overlap consequently is seen to increase until thermal equilibrium with the floor is reached (Fig. 5c). Another interesting aspect, as a consequence of the increase in the overlap, is the increment of the contact area (Fig. 5d), of about 63%, if compared to the area when thermal softening is not considered. This implies an increase in the amount of conduction heat flow between both objects, as it can be seen in Fig. 5e. Therein, a reference line at $t = 8$ s is plotted in the graph, for which the temperature of the particle is seen to be about 7% higher than that in the case without thermal softening. Also, with thermal softening thermal equilibrium is reached faster than in the case without softening (~ 12 s against ~ 18 s). With regard to the contact force, the change in elastic modulus and overlap would make one to expect that the contact force also varies in time; however, it is seen from the graph in Fig. 5f that this does not happen: after mechanical equilibrium is attained (this occurs very rapidly at the beginning and cannot be seen from the adopted graph scale), the force is perfectly constant in time, with a value of 1.23×10^{-4} N. It turns out that the decrease in stiffness is exactly compensated by the increase in the overlap, and the force remains constant thereby. Indeed, this is consistent with static equilibrium arguments, since the only external force acting upon the particle is the gravity force, which is constant. The time-step size adopted in this simulation was $\Delta t = 2 \times 10^{-5}$ s whereas the final time was $t = 40$ s.
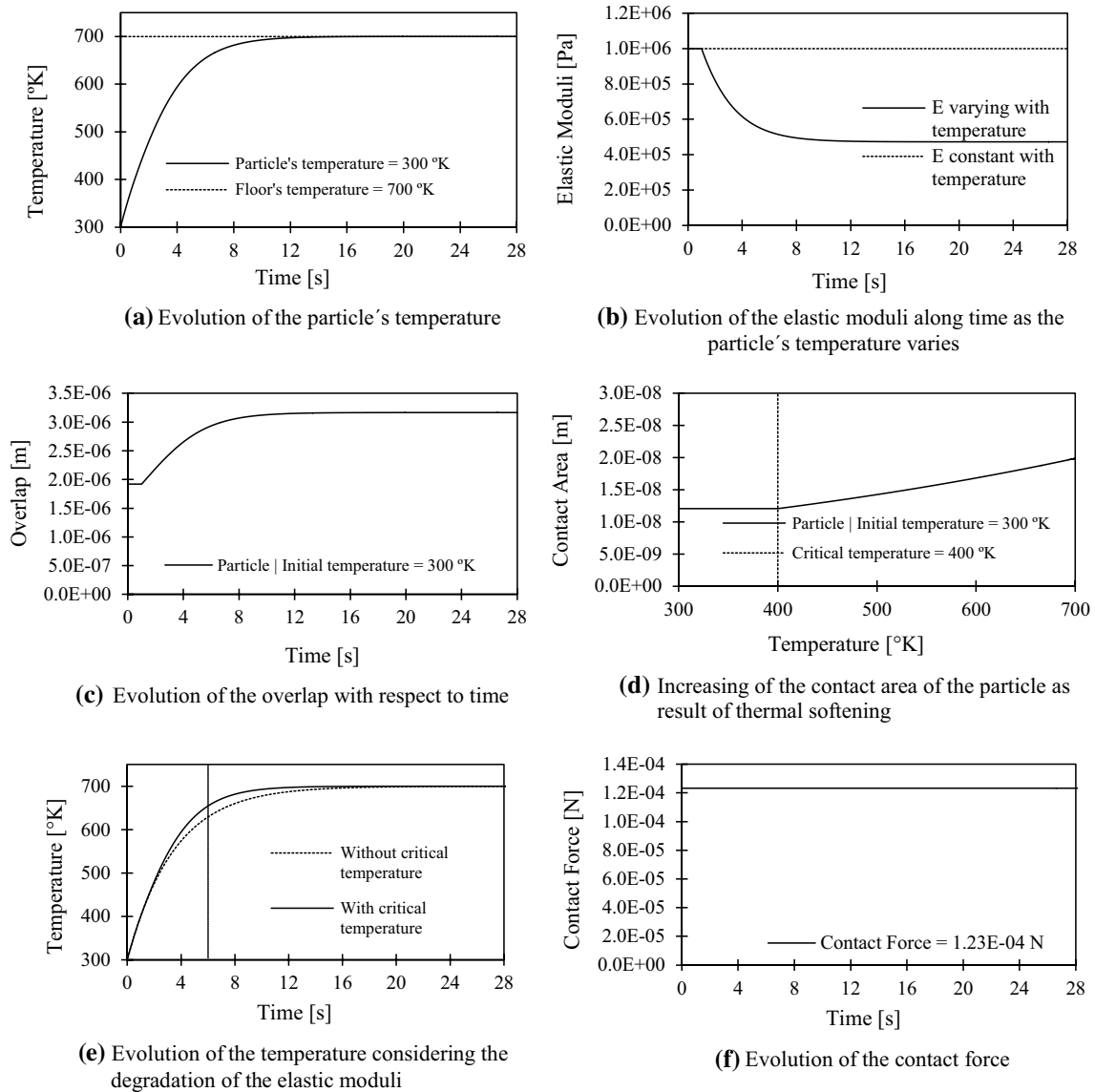
(a) Evolution of the particle´s temperature

(b) Evolution of the elastic moduli along time as the particle´s temperature varies

(c) Evolution of the overlap with respect to time

(d) Increasing of the contact area of the particle as result of thermal softening

(e) Evolution of the temperature considering the degradation of the elastic moduli

(f) Evolution of the contact force

Fig. 5 Example 5.1: interaction between a particle and a thermal base. Analysis results

Fig. 6 Heated and vibrated extended granular medium. Problem definition. The initial temperature of the particles is 300 K

$y(t) = A\sin(\omega t)$

triangular piling

11.9 mm

300 mm
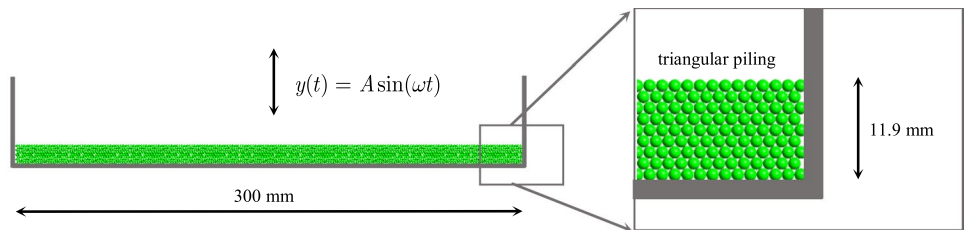
5.2 Heated and vibrated extended granular medium

This example has been originally proposed by Campello [3], however without consideration of heat. At the time, the author was interested in the purely mechanical part of the problem, namely the onset of surface instabilities followed by the formation of well-marked surface waves. This interesting phenomenon may be observed if an extended (i.e., shallow) granular stack is vibrated vertically under certain frequencies. It has been studied through physical experiments by Duran [8] and Clément et al. [25], among others,

and their results were numerically reproduced in [3]. Here, instead, we want to analyze a thermo-mechanical version of the problem, by heating up the granular medium while it is being vibrated, with the aim to investigate the evolution of its thermal states and the role of conduction and convection. Accordingly, nine layers of particles with diameter 1.5 mm and initial temperatures 300 K are disposed at the bottom of a rectangular cell of 300 mm width, as shown in Fig. 6 (the same setting as in the original example). The layers are piled in a regular triangular arrangement, such that the total height of the stack at rest is 11.9 mm. The problem is mounted in a bi-dimensional setting, as to facilitate visualization of results. The cell is shaken vertically according to the displacement function $y(t) = A \sin(\omega t)$, with given amplitude A and angular frequency ω. A normalized acceleration measure, $\Gamma = A\omega^2/g$ (with $g = 9.8$ m/s^2 as the gravity acceleration), is taken as a control parameter. At $t = 0$, the cell walls are given an initial temperature of 1000 K, which is then held constant throughout the simulation. The air's temperature, in turn, is taken as 273 K. Other data are as follows:

- Mass-density of the particles: $\rho_i = 2700$ kg/m^3;
- Elastic properties of the particles: $E_i = 700$ MPa and $\nu_i = 0$;
- Friction and rolling resistance coefficients between particles: $\mu_s = \mu_d = 0.5$ and $\mu_r = 0.01$;
- Friction and rolling resistance coefficients between particles and cell walls: $\mu_s = \mu_d = \mu_r = 0$;
- Contact, friction and rolling resistance damping rates: $\xi^{con} = \xi^{fric} = 0.16$ and $\xi^{rol} = 0.01$;
- Thermal properties of the particles: $k_i = 500$ W/m K and $C_i = 5$ J/kg K;
- Thermal properties of air: $k_{air} = 0.025$ W/m K and $C_{air} = 1000$ J/kg K;
- Normalized acceleration parameter: $\Gamma = 3.4$;
- Total number of particles: $N_P = 1796$;
- Time-step size: $\Delta t = 5 \times 10^6$ s.

Radiative effects and thermal softening are not considered (this allows us to concentrate solely on the effects of conduction and convection here). Figure 7 shows two sequences of snapshots as obtained with our simulation for the case with an excitation frequency of $f = 7.8$ Hz (which corresponds to a shaking amplitude of $A = 13.9$ mm). The left sequence is obtained by considering both conduction and convection, whereas for the right one the convection contribution is turned off. One can see that heat transfer through convection is particularly dominant here, not allowing the particles to heat up significantly even after they have made tens of thousands of contacts with the walls at $t = 60$ s. If convection is not considered, the particles' temperatures steadily grow as the bottom and lateral layers are heated due to multiple contacts with the walls, and from them the other layers are heated through inter-particle conduction. The particles are clearly seen to approach the walls' temperature with increasing time. Figure 8 displays the corresponding results for the case with an excitation frequency of $f = 12$ Hz (which corresponds to a shaking amplitude of $A = 5.9$ mm). The same overall behavior is observed, except that here the waves have a rather smaller height, and as consequence the heat transfer paths are different, leading to a different exchange of heat between particles and between particles and the environment. For this reason, the temperature distributions are slightly different as compared to the previous case.

5.3 Conduction through a 3D particle assembly

We consider here a three-dimensional particle assembly consisted of $N_P = 10000$ particles randomly packed under gravity within a cubic box, subjected to a temperature gradient of 700 K in its x direction as depicted in Fig. 9, top part. The box has side dimensions of 0.1 m, whereas the particles have radii following a Gaussian distribution with mean $\bar{r} = 3.0$ mm and standard deviation 0.667 mm (the distribution is truncated at three standard deviations from the mean). The volume fraction of particles within the assembly is 0.54. The thermal gradient is enforced by holding the temperatures of the two opposite walls of the box in the x direction at 1000 K and 300 K indefinitely, respectively, with the particles' initial temperatures being set at 300 K. By releasing the system at $t = 0$ and computing the evolution of heat flow over time, we are able to ascertain the effective (i.e., bulk) thermal conductivity of the assembly, which is obviously not the same of the individual conductivities of the constituent particles. Convection and radiation are not considered as to isolate the conduction problem and allow for a better estimate of the effective response. Other data are as follows:

- Particles' thermal properties: $k_i = 100$ W/m K and $C_i = 100$ J/kg K;
- Particles' mass-density: $\rho_i = 1000$ kg/m^3;
- Particles' elastic properties: $E_i = 1$ MPa (no thermal softening) and $\nu_i = 0.3$;
- Friction and rolling resistance coefficients between particles: $\mu_s = \mu_d = 0.05$ and $\mu_r = 0.2$;
- Friction and rolling resistance coefficients between particles and cell walls: $\mu_s = \mu_d = \mu_r = 0$;
- Contact, friction and rolling resistance damping rates: $\xi^{con} = \xi^{fric} = 1.0$ and $\xi^{rol} = 0.2$;
- Pack generated through a random sequence addition method (Campello and Cassares [26]);
- Time-step size: $\Delta t = 2 \times 10^4$ s.

Figure 9 shows snapshots of the system's configuration at selected time instants as obtained with our simulation (sequence is from left to right, top to down). Thermal
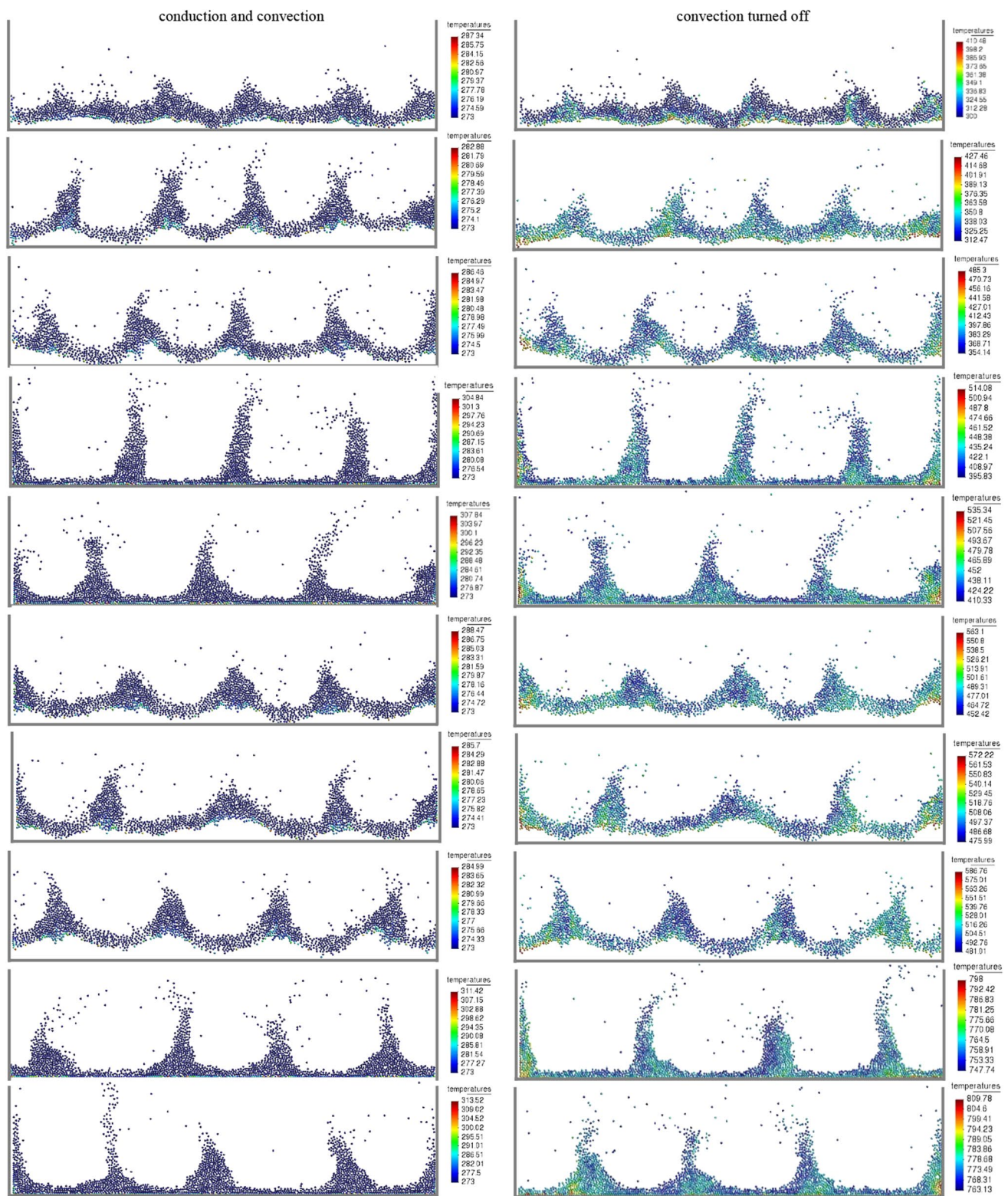
Fig. 7 Heated and vibrated extended granular medium. Simulation results for the case with $f = 7.8$ Hz. Left sequence considers both conduction and convection; right sequence has convection turned off.

Snapshots (from top to down) are taken at $t = 1$ s, 3 s, 6 s, 8 s, 10 s, 13 s, 20 s, 30 s, 40 s and 60 s, respectively
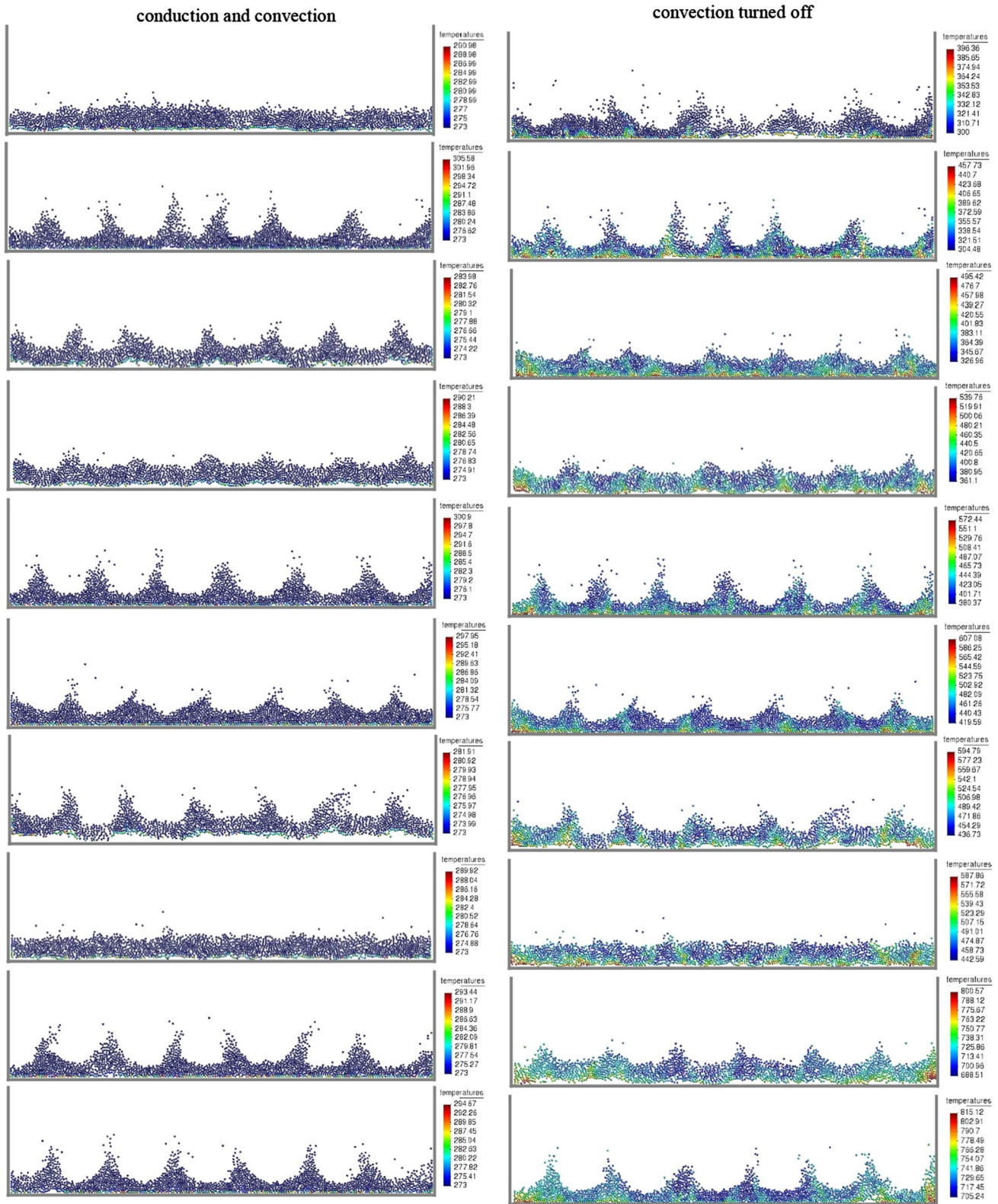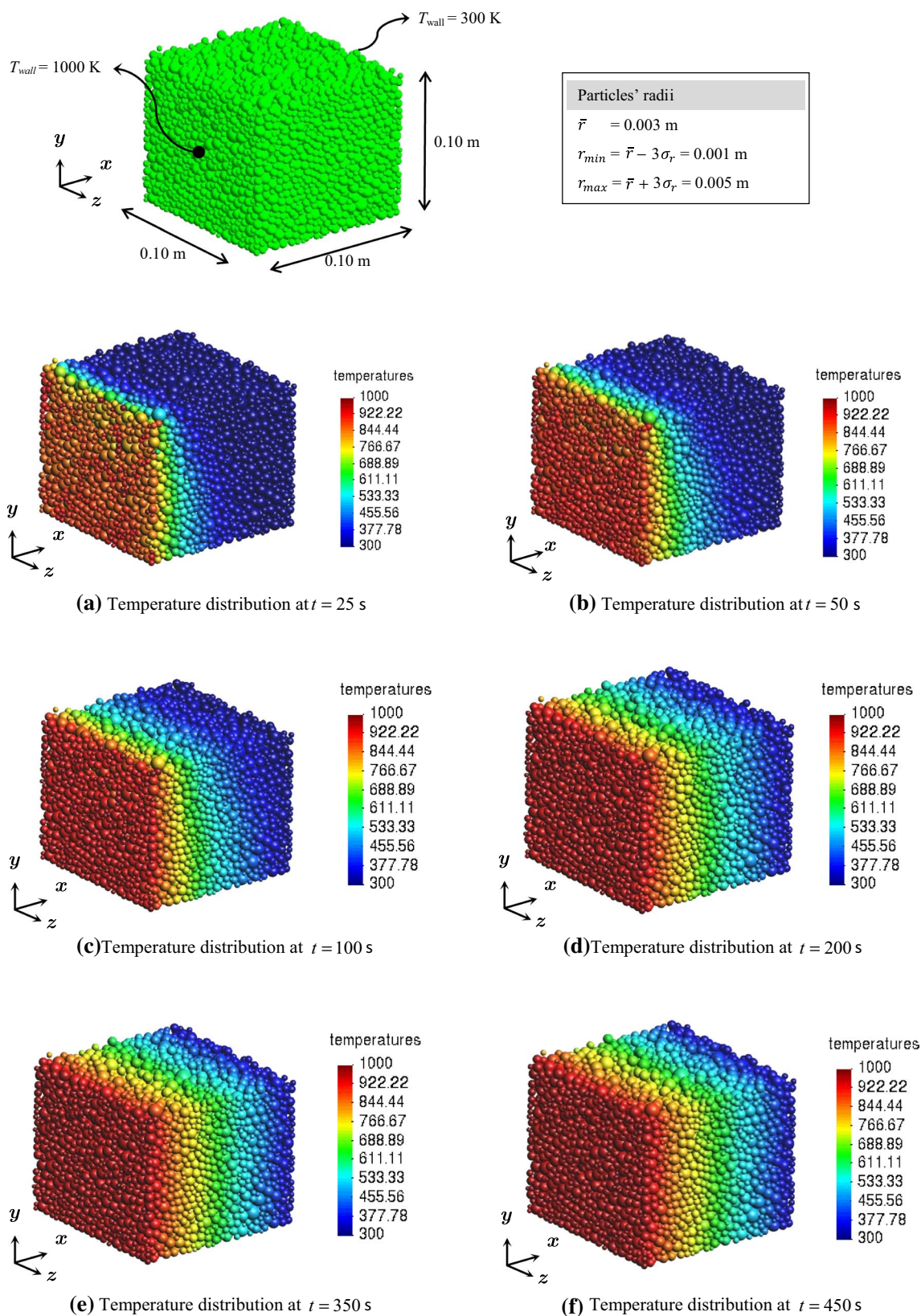
Fig. 8 Heated and vibrated extended granular medium. Simulation results for the case with $f = 12$ Hz. Left sequence considers both conduction and convection; right sequence has convection turned off. Snapshots (from top to down) are taken at $t = 1$ s, 3 s, 6 s, 8 s, 10 s, 13 s, 20 s, 30 s, 40 s and 60 s, respectively

(a) Temperature distribution at $t = 25$ s

(b) Temperature distribution at $t = 50$ s

(c) Temperature distribution at $t = 100$ s

(d) Temperature distribution at $t = 200$ s

(e) Temperature distribution at $t = 350$ s

(f) Temperature distribution at $t = 450$ s

Fig. 9 Conduction through a 3D particle assembly. Simulation results. Sequence is from left to right, top to down

equilibrium is reached at around $t \approx 350$ s, wherein the particles' temperatures no longer change significantly between consecutive time steps. From the thermal field thus obtained, the total heat that is provided to the system until then (ΔQ) may be computed by summing up the change in the particles' individual thermal energies w.r.t. the initial configuration, i.e., $\Delta Q = \sum m_i C_i \Delta \theta_i$. The effective conductivity of the assembly in the x-direction, then, may be obtained by $k^* = \Delta Q/(\nabla T A \Delta t)$, where $\nabla T = 700/0.1 = 7000$ K/m is the applied thermal gradient, $A = 0.1 \times 0.1 = 0.01$ m^2 is the cross-sectional area to the flow and $\Delta t = 350$ s is the time interval considered. From this, it follows that $k^* = 6.2$ W/m K. In order to check the consistency of this result, let us resort to the well-known Hashin–Shtrikman bounds (Hashin and Shtrikman [27–29]) on effective responses for two-phase solid mixtures. For linear heat transfer applications, for a mixture of two isotropic materials, each with known thermal conductivities k_1 and k_2 and volume fractions v_1 and v_2, the bounds for the effective bulk conductivity are

$$k_1 + \frac{v_2}{\frac{1}{k_2-k_1} + \frac{1-v_2}{3k_1}} \leq k^* \leq k_2 + \frac{1-v_2}{\frac{1}{k_1-k_2} + \frac{v_2}{3k_2}}, \tag{48}$$

wherein it is implicitly assumed that $k_2 \geq k_1$. Phase 1 is the matrix (in our case, void) material, whereas phase 2 is the particle one. Provided that the volume fractions and constituent conductivities are the only known information about the mixture's microstructure, the Hashin–Shtrikman expressions are the tightest bounds for the overall effective responses of two-phase media, where both constituents are isotropic. One should notice that the lower bound is more accurate for mixtures composed of highly conductive particles surrounded by a lowly conductive matrix (which is the case here), whereas the upper bound is more accurate for mixtures of a highly conductive matrix surrounding lowly conductive particles. For the conductivities adopted here ($k_1 = 0$ and $k_2 = 100$ W/m K), the above expression renders a lower bound of $k^{*,-} = 0$, and an upper bound of $k^{*,+} = 44.6$ W/m K. This is entirely consistent with the value derived from our simulation: not only our numerical estimation lies within the bounds, but also it is much closer to the lower (more accurate) one. One additional explanation to the fact that the assembly's effective conductivity shall be closer to the lower bound here is that the particles, though occupying roughly 54% of the assembly's total volume, interact with their neighboring ones through minute contact areas, such that the conductivity paths, although existing within the entire assembly, are of very small cross-sectional size, thus affecting the conduction rates severely. To further check the consistency of our proposed scheme, we have run one additional simulation of the assembly, now considering thermal softening of the elasticity modulus, in an attempt to increase the particles' contact areas and thus improve the overall

Table 1 Laser-sintering of a bed of particles. Values used in the simulation

No.	Parameter	Values
1	Particle's diameter (mean, std. dev)	1.0 mm, 0.1 mm
2	Number of particles	6401
3	Particles' initial temperatures	373 K
4	Particles' degrading temperature	700 K
5	Particles' material density	7800 kg/m^3
6	Particles' elastic modulus and Poisson coeff.	200 GPa and 0.3
7	Particles' friction and rolling resistance coeffs.	0.1
8	Particles' damping rates	1.0
9	Bed's lateral dimensions	40 mm × 40 mm
10	Laser power	1000 W
11	Laser beam diameter	10 mm
12	Laser beam horizontal velocity	0.1 m/s
13	Particles' thermal conductivity	60 W/m K
14	Particles' heat capacity	600 J/kg K

conductivity of the assembly. By considering a critical temperature of $\theta^* = 300$ K, the new thermal field obtained at the time of thermal equilibrium (i.e., when the particles' temperatures no longer change significantly between consecutive time steps) leads to $k^* = 7.4$ W/m K. This is entirely consistent, since it is higher than the first estimate, however still closer to the lower bound. It is important to mention that the increase in k^* in this case is indeed expected to be small, since the softening adopted is rather mild. More pronounced increases may be accomplished by softening the particles more severely. At any rate, any estimate to the effective conductivity in this problem shall be closer to the lower bound. The proposed methodology provides a simple and useful way to ascertain the effective thermal conductivity of dry powders and other particulate media used in industrial processes and advanced engineering applications. A similar approach to effective responses, though in the rather different context of particle infiltration into porous media, has been developed recently by Zohdi and Campello [30].

5.4 Laser-sintering of a bed of particles

This example has been proposed by Ganeriwala and Zohdi [31]. Here, we analyze it with a few slight modifications: we consider Hertz-based contact, consistent stick–slip friction, consistent rolling resistance, as well as convection, radiation and thermal softening of the particles' elasticity modulus (instead of [31] 's no convection, no radiation and no thermal softening), but with no phase transformation. To better highlight the effects of these phenomena, the particles' diameters and bed's lateral dimensions have been changed here in comparison with Ganeriwala and Zohdi's original example.
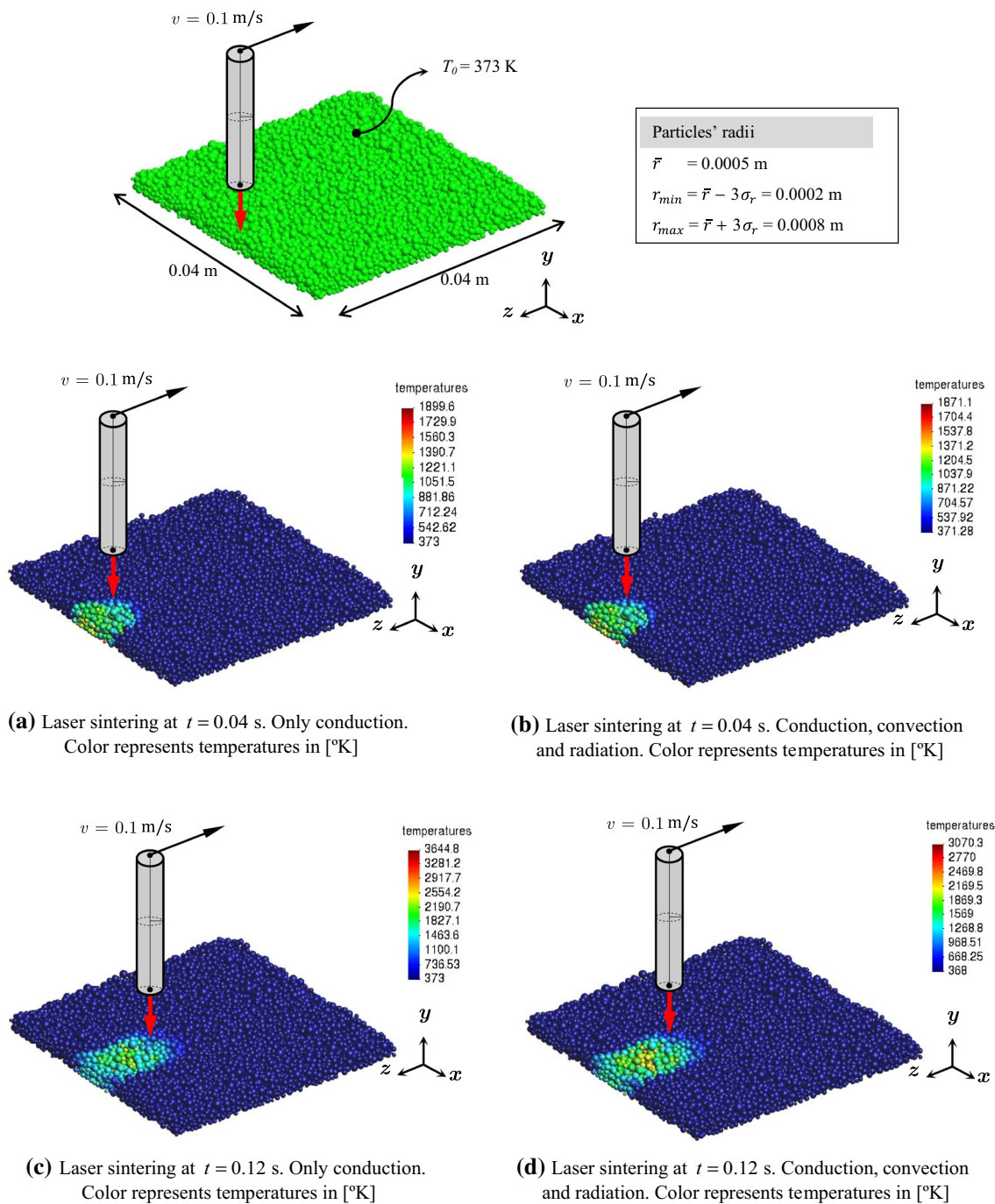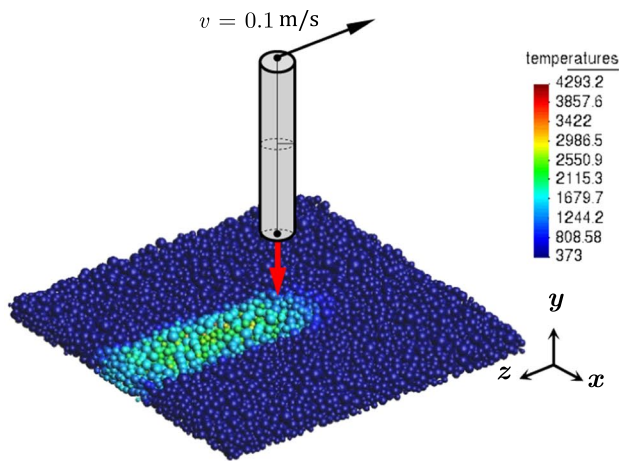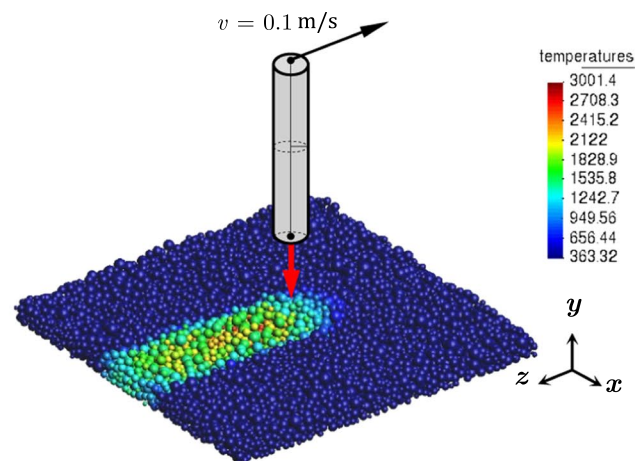
(a) Laser sintering at $t = 0.04$ s. Only conduction. Color represents temperatures in [°K]

(b) Laser sintering at $t = 0.04$ s. Conduction, convection and radiation. Color represents temperatures in [°K]

(c) Laser sintering at $t = 0.12$ s. Only conduction. Color represents temperatures in [°K]

(d) Laser sintering at $t = 0.12$ s. Conduction, convection and radiation. Color represents temperatures in [°K]

Fig. 10 Laser-sintering of a bed of particles. Problem definition and simulation results up to $t = 0.12$ s. Left sequence considers only conduction; right sequence considers conduction, convection and radiative effects

Accordingly, a bed of metallic particles whose properties are summarized in Table 1 is heated from above by a high-intensity laser beam, as shown in Fig. 10, top part. The laser moves in the horizontal z-direction at a constant speed of 0.1 m/s, as to heat the particles and promote their rapid sintering. Its properties are shown in Table 1. The beam's intensity is assumed to be uniform throughout its cross-sectional area. The environment's temperature is assumed to be 273 K. Considering that the particles are very stiff, a small time-step size of $\Delta t = 5 \times 10^{-7}$ s is adopted. The total simulation time is $t_F = 0.5$ s. Figures 10 and 11 show a sequence of screenshots at selected time instants as obtained with our simulation. The left sequence refers to the simulation considering only conduction heat transfer, whereas the right
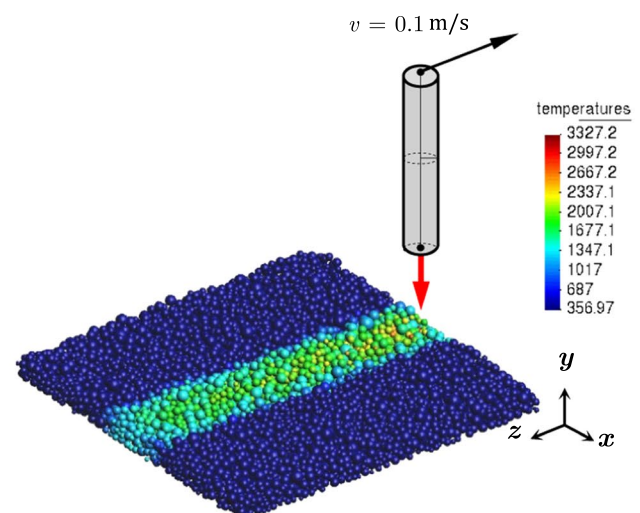
(a) Laser sintering at $t = 0.24$ s. Only conduction. Color represents temperatures in [ºK]

(b) Laser sintering at $t = 0.24$ s. Conduction, convection and radiation. Color represents temperatures in [ºK]
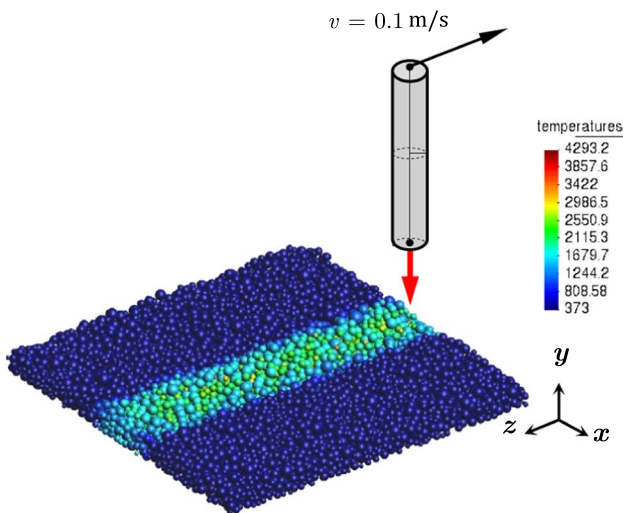
(c) Laser sintering at $t = 0.416$ s. Only conduction. Color represents temperatures in [ºK]

(d) Laser sintering at $t = 0.416$ s. Conduction, convection and radiation. Color represents temperatures in [ºK]

Fig. 11 Laser-sintering of a bed of particles. Simulation results from $t = 0.24$ to $t = 0.416$ s. Left sequence considers only conduction; right sequence considers conduction, convection and radiative effects

sequence considers conduction, convection and radiative effects. At $t = 0.24$ s, for example, it can be seen that the average temperature of the particles (considering only those that have been targeted by the beam) for the case with only conduction is 2986 K, whereas for the case with conduction, convection and radiation it is 2121 K—a difference of about 41%. As for the maximum temperatures, a difference of about the same order (43%) is observed between both cases. Contrary to Ganeriwala and Zohdi [31], wherein the particles were of a smaller average size, here the convection and radiative contributions play a very significant role. The process performance may be severely impacted if they

are not taken into account in the model. Another interesting aspect that can be seen in both cases is that particles located near the boundaries of the beam's path-length heat up less than those further within the path, due to conduction with the cooler neighboring particles that have not been targeted by the beam. At any rate, irrespective of these observations, we remark that, due to the high temperatures experienced by the particles here, a more rigorous approach to this problem would require one to incorporate phase transformation effects and, occasionally, adhesion forces. This is already under development by the authors.

6 Conclusions

Discrete particle systems consisted of thermo-mechanically active particles are widely observed in many industrial processes and engineering applications. This is the case of (but is not restricted to) modern advanced manufacturing and state-of-the-art civil construction, wherein the controlled heating (and further processing) of particles such as sintering powders and functionalized cementitious materials is critical. In order to have a reliable and fairly accurate representation of the behavior of such systems under external (thermal and mechanical) excitations, a multiphysical description is required. The purpose of this work was to present a multiphysics computational model for the simulation of such discrete particle systems. We find the model to be reasonably simple and straightforward to be implemented by engineers and analysts interested in the field. We aimed to enable a direct design and analysis tool with which analysts and engineers may assess the overall system's response upon given external excitations, detecting general trends, identifying the relevance of certain parameters (and their subsequent impact upon the system's behavior), drawing what-if scenarios and thereby reliably improving process performance. The model proved to work very well for the purposes envisioned, as demonstrated in our numerical examples. This truly motivates us to pursue in its extension and improvement. In this regard, incorporation of more complex phenomena such as adhesion forces, chemical reactions, heat generation through inelastic collisions as well as phase transformation is currently under development by the authors. Likewise, the implicit version of the numerical solution scheme is under work. All these advancements over the present model shall appear soon in a forthcoming paper. We believe that simple, consistent particle models of the type as shown here may be a useful tool to the modeling of discrete particle systems that are consisted of thermo-mechanically active particles and, in a broader sense, many other discrete systems wherein multiphysical effects may be relevant.

References

1. Vargas-Escobar WL (2002) Discrete modeling of heat conduction in granular media. Doctoral thesis, School of Engineering—University of Pittsburgh, Pittsburgh
2. Radjaï F, Dubois F (2011) Discrete numerical modeling of granular materials. Wiley, Hoboken
3. Campello EMB (2018) A computational model for the simulation of dry granular materials. Int J Nonlinear Mech 106:89–107
4. Campello EMB (2015) A description of rotations for DEM models of particle systems. Comput Part Mech 2:109–125
5. Campello EMB (2016) Um modelo computacional para o estudo de materiais granulares. Habilitation thesis, Escola Politécnica da Universidade de São Paulo, São Paulo
6. Zohdi T (2012) Dynamics of charged particulate systems: modeling, theory and computation. Springer, New York
7. Zohdi T (2014) Additive particle deposition and selective laser processing—a computational manufacturing framework. Comput Mech 54:171–191
8. Duran J (1997) Sands, powders and grains: an introduction to the physics of granular matter. Springer, New York
9. Bicanic N (2004) Discrete element methods. In: Stein E, Borst RD, Hughes TJ (eds) Encyclopedia of computational mechanics, volume 1: fundamentals, vol 1. Wiley, Chichester, pp 1–33
10. Zhu HP, Zhou ZY, Yang RY, Yu AB (2008) Discrete particle simulation of particulate systems: a review of major applications and findings. Chem Eng Sci 63:5728–5770
11. Zhu HP, Zhou ZY, Yang RY, Yu AB (2007) Discrete particle simulation of particulate systems: theoretical developments. Chem Eng Sci 62:3378–3392
12. O'Sullivan C (2011) Particle-based discrete element modeling: geomechanics perspective. Int J Geomech 11:449–464
13. Thornton C, Cummins SJ, Cleary PW (2013) An investigation of the comparative behaviour of alternative contact force models during inelastic collisions. Powder Technol 233:30–46
14. Radjai F, Roux J-N, Daouadji A (2017) Modeling granular materials: century-long research across scales. J Eng Mech 143(4):04017002-1–04017002-20
15. Zohdi TI (2018) Modeling and simulation of functionalized materials for additive manufacturing and 3D printing: continuous and discrete media. Springer, New York
16. Gibson I, Rosen D, Stucker B (2015) Additive manufacturing technologies: 3D printing, rapid prototyping, and direct digital manufacturing. Springer, New York
17. Johnson KL (1985) Contact mechanics. Cambridge University Press, Cambridge
18. Campello EMB, Zohdi T (2014) A computational framework for simulation of the delivery of substances into cells. Int J Numer Methods Biomed Eng 30:1132–1152
19. Zohdi T (2014) A direct particle-based computational framework for electrically-enhanced thermo-mechanical sintering of powdered materials. Math Mech Solids 19(1):93–113
20. Feng YT, Han K, Owen DRJ (2009) Discrete thermal element modeling of heat conduction in particle systems: pipe-network model and transient analysis. Powder Technol 193:248–256
21. Yan C, Jiao Y-Y (2019) A 2D discrete heat transfer model considering the thermal resistance effect of fractures for simulating the thermal cracking of brittle materials. Acta Geotech. https://doi.org/10.1007/s11440-019-00821-x
22. Yan C, Ren Y, Yang Y (2019) A 3D thermal cracking model for rockbased on the combined finite-discrete element method. Comput Part Mech. https://doi.org/10.1007/s40571-019-00281-w
23. Whitaker S (1972) Forced convection heat transfer correlations for flow in pipes, past flat plates, single cylinders, single spheres, and flow in packed beds and tube bundles. AIChE J 18:361371
24. Campello EMB (2020) Effect of particle spin on the spatio-thermal distribution of incandescent materials released from explosions. J Braz Soc Mech Sci Eng 42:40. https://doi.org/10.1007/s40430-019-2123-y
25. Clement E, Vanel L, Rajchenbach J, Duran J (1996) Pattern formation in a vibrated granular layer. Phys Rev E 53(3):2972–2975
26. Campello EMB, Cassares KR (2016) Rapid generation of particle packs at high packing ratios for DEM simulations of

granular compacts. Latin Am J Solids Struct 13:23–50. https://doi.org/10.1590/1679-78251694

27. Hashin Z, Shtrikman S (1962) On some variational principles in anisotropic and nonhomogeneous elasticity. J Mech Phys Solids 10:335–342

28. Hashin Z, Shtrikman S (1963) A variational approach to the theory of the elastic behaviour of multiphase materials. J Mech Phys Solids 11:127–140

29. Hashin Z (1983) Analysis of composite materials: a survey. ASME J Appl Mech 50:481–505

30. Zohdi TI, Campello EMB (2019) On pressurized functionalized particle-laden fluid infiltration into porous media. Int J Multiscale Comput Eng 17(2):223–237

31. Ganeriwala R, Zohdi TI (2014) Multiphysics modeling and simulation of selective laser sintering manufacturing processes. In: Procedia CIRP 14 (6th CIRP international conference on high performance cutting, HPC2014), Berkeley, USA